Validation of Elastic Wave Measurements of Rock Fracture Compliance Using Numerical Discrete Particle Simulations

M. Möllhoff (1) and C.J. Bean (1,2)

(1) Seismology and Computational Rock Physics Laboratory

UCD School of Geological Sciences

University College Dublin, Belfield, Dublin 4, Ireland

email: martin.moellhoff@ucd.ie

(2) Complex and Adaptive Systems Laboratory (CASL)

University College Dublin, Belfield, Dublin 4, Ireland

Abstract

We test various methods of quantifying the compliance of single and multiple rock fractures from synthetic ultrasonic data. The data are generated with a 2D Discrete Particle Scheme which has previously been shown to treat fractures in agreement with linear-slip theory. Studying single fractures, we find that delays derived from peak amplitudes do not correspond to group delays, as might be expected. This is due to waveform distortion caused by the frequency-dependent transmission across the fracture. Instead the delays correspond to an expression for phase delays, which we derive from linear-slip theory. Phase delays are a unique function of compliance, whereas group delays are non-uniquely related to compliance. We believe that this property of group delays has hindered the wider application of deriving fracture compliances from travel times. We further show that transmission coefficients derived from waveform spectra yield more accurate fracture compliances than those obtained from ratios of signal peak amplitudes. We also investigate the compliance of a set of parallel fractures. Fracture compliance can only be determined from transmission coefficients if the fracture spacing is so large that the first arriving pulse is not contaminated by reverberations. In the case of contamination direct measurement of group or phase delays is not practical. However, we demonstrate that in such cases of strong waveform distortion the Coda Wave Interferometry method is very effective for determining relative fracture compliance. First break

delays in the fracture set data are related to those observed in single fracture simulations. This means that fracture set compliance can be estimated from first break data if used together with numerical simulations.

Keywords

fracture, compliance, time delay, transmission coefficient, coda wave interferometry.

Introduction

Fracture compliance plays an important role in various geophysical applications, e.g. ultrasonic laboratory rock studies, rock damage and stability investigations, hydrocarbon recovery, fault zone studies, CO_2 and nuclear waste leakage monitoring and also in engineering applications, e.g. nondestructive testing of bonded materials. The aim of this work is to further the understanding of how, in practice, to quantify fracture compliance from ultrasonic data. Our approach is to apply a range of methods for measuring compliance to numerical simulation data from fractured rock models. The true compliances are known *a priori*, hence the accuracy of the analysis methods can be tested. Results are also compared with analytical work by Schoenberg (1980), which is often referred to as the theory of linear-slip interfaces. In this theory fractures are considered as imperfect interfaces across which stress is continuous but displacement is discontinuous. Linear-slip theory relates fracture compliance directly with the frequency dependent transmission coefficient and time delay characteristics of planar fractures. This theory has been successfully tested with ultrasonic laboratory experiments by Pyrak-Nolte, Myer and Cook (1990a), Hsu and Schoenberg (1993) and others. Throughout this paper we consider the normal fracture compliance Z defined as the ratio between the normal displacement discontinuity Δu caused by a normal stress σ

$$Z = \frac{\Delta u}{\sigma} \tag{1}$$

We model fractures numerically with the Discrete Particle Scheme (Toomey and Bean 2000). The scheme consists of a 2-D lattice of bonded circular particles that interact through spring-like bonds. Employing the Discrete Particle Scheme we generate synthetic ultrasonic waveforms. Various authors have demonstrated that the numerical discrete particle modelling of individual fractures is in accordance with linear-slip theory (e.g. Cai and Zhao (2000); Toomey, Bean and Scotti (2002)). While these authors studied effects on monochromatic signals, here we consider the more general case of non-monochromatic signals. This is important because sources are usually non-monochromatic and because the transmission characteristics and the time delay caused by a fracture are frequency dependent. Comparing transmission coefficients derived from peak amplitudes and from signal spectra we find that only the latter result in fracture compliances that agree accurately with the analytical solution of linear-slip theory. We also investigate the compliance dependency of time delays derived from maxima of signal envelopes and from peak amplitudes. While the former match the analytical solution for group delays, the latter fit an analytical solution for phase delays. This is an important observation for the practical determination of fracture compliance from real data because linear-slip theory demonstrates that phase delays are uniquely

related to fracture compliance while group delays are not.

Because rock fractures often occur in clusters and cannot be treated in isolation we also consider sets of parallel fractures. Effective and equivalent medium models are often employed to simulate seismic wave propagation in fractured rock assuming wavelengths are much larger than fracture spacing or fracture length (e.g. Schoenberg and Sayers (1995)). For seismic wavelengths smaller than or comparable to fracture spacing and fracture length, reverberation and scattering occurs and the correct response of the medium can only be obtained by modelling discrete fractures (Myer *et al.* (1995); Willis *et al.* (2006); Prioul *et al.* (2007); Worthington (2007)). We apply the Discrete Particle Scheme to systems of parallel fractures with spacings covering both, relatively large and relatively small scales. In order to focus on the effects of fracture compliance and spacing on transmission coefficients and travel-time delays, we use an isotropic background and parallel, effectively infinitely wide, equidistant fractures. We find that the observed transmission coefficients only agree with an analytical solution that assumes non-interaction between fractures, i.e. the fracture spacing is large compared to the dominant signal wavelength. This is in agreement with other studies (e.g. O'Doherty and Anstey (1971); Cai and Zhao (2000)) and prohibits the quantification of compliance of densely spaced fracture sets from transmission coefficients. While we find that group and phase delays are also generally unsuited to quantify compliance, first break delays are simply multiples of single fracture first

break delays.

If fracture induced signal distortion is too strong to allow for precise first break picking or if reverberations cause signal envelopes to overlap, the Coda Wave Interferometry method (Snieder 2002) can be employed to determine time delays. Time delays derived with this method are shown to be consistent with group delays.

Theory and Methods

The numerical Discrete Particle Scheme

The simulations in this study are modelled with the Discrete Particle Scheme (Toomey and Bean 2000). The scheme consists of a 2-D hexagonal lattice of equally sized bonded discs with a thickness of 1m, see Fig. 1. The bond stiffnesses are normal to the particle contact planes with zero tangential stiffness and their values are computed according to equation 3 in Toomey and Bean (2000). The Poisson's ratio of such a hexagonal particle arrangement is 0.25 (Hoover, Ashurst and Olness 1974), which is a typical value for crustal rocks. The particles interact according to a linear force-displacement rule with no damping. Attenuation can be added to the Discrete Particle Scheme (see O'Brien (2008)), but to isolate the attenuation effects of the modelled fractures we consider an elastic

medium. The fracture compliance is controlled by lowering the bond stiffness between particles on either side of a fracture interface, see Fig. 1. The resulting elastic fracture properties are in agreement with linear-slip theory as shown by Toomey *et al.* (2002). The linear-slip theory has been validated with physical laboratory experiments by various authors (e.g. Pyrak-Nolte *et al.* (1990a)). Also Lubbe and Worthington (2006) employed the Discrete Particle Scheme successfully to replicate seismic data from crosshole experiments. We thus assume that the Discrete Particle Scheme realistically models ultrasonic waves in fractured rock. The computational demands for the large number of required simulations in this study did not allow us to employ 3D model simulations. However, a preliminary comparison with the 3-D lattice scheme by O'Brien and Bean (2004) showed that time delays derived from the early part of wave packages are not effected by the 2-D or 3-D nature of the numerical model.

The simulation parameters in this work resemble typical ultrasonic laboratory rock experiments with a model height of 8cm, a width of 4cm and a Ricker wavelet source function with a central frequency of 1 MHz. The simulated medium has a density of 2575 kg/m^3 and a p-velocity of 5590 m/s, which is within the typical range for granite (Jaeger, Cook and Zimmerman 2007). Granite has been choosen because it is widely used in ultrasonic laboratory experiments and is less attenuative than for example sedimentary rocks. All simulations are run with a particle diameter of 0.1mm because numerical dispersion is neglegible at this relativly

small size.

The compliances of the modelled fractures are determined with quasistatic compression experiments, see section 'Quantification of Fracture Compliance'. We consider compliances in a range of 0.01 - 2.14 x 10^{-13} m/Pa by lowering bond stiffnesses to values in a range from 0.5% to 60% of the rock matrix. This compares with ranges of 0.2 - 2.20 x 10^{-13} m/Pa (Pyrak-Nolte, Cook and Myer 1987), 0.07 - 3.57 x 10^{-13} m/Pa (Pyrak-Nolte *et al.* 1990a) and 0.01 - 0.32 x 10^{-13} m/Pa (Lubbe *et al.* 2008) observed in ultrasonic laboratory experiments.

We investigate the interaction of dynamic waves with fractures by applying a planar vertical source along the entire top of the model and sampling displacement data at the bottom. In order to allow for a direct comparison with analytical solutions we consider non-reflective boundary conditions for plane waves travelling parallel to the side boundaries of the model. This is achieved by a mirroring condition for particles on the side boundaries by setting their forces equal to those experienced by their direct neighbours towards the model interior. The top and bottom of the model act as free surfaces. For the single fracture simulations we place a plane horizontal fracture across the centre of the model, see Fig. 1. For the simulations of fracture sets we place five plane horizontal, equally compliant, equidistant fractures in the model, see Fig. 2.

Time Delays in Fractured Media

Many ultrasonic and seismological analysis techniques rely on the measurement of travel times or differences between travel times, called time delays. Papoulis (1962) and Scherbaum (2002) define different types of time delays by considering a general filter with a frequency response function H, where ω is the angular signal frequency, Θ the signal phase and i is $\sqrt{-1}$

$$H(i\omega) = |H(i\omega)| \cdot e^{i\Theta(\omega)} \tag{2}$$

Applying the filter for example to a harmonic signal $A \cdot sin(\omega t)$ gives the output $A \cdot |H(i\omega)| \cdot sin(\omega t + \Theta(\omega))$, where $\Theta(\omega)$ is the phase by which the signal is advanced (in radians) and $A \cdot |H(i\omega)|$ is the amplitude of the output. The frequency ω of the signal remains unchanged. The phase delay t_{ph} corresponding to the phase shift $\Theta(\omega)$ is defined as

$$t_{ph}(\omega) = -\frac{\Theta(\omega)}{\omega} \tag{3}$$

The delay between the signal envelopes (i.e. the pulse's centre of gravity) gives the group delay defined as

$$t_g(\omega) = -\frac{d\Theta(\omega)}{d\omega} \tag{4}$$

The concepts of phase and group delay apply only to narrow-band signals (Papoulis 1962). A common approach to determine time delays in practice is to pick the onset time of a signal, often called first break or first pick. If a medium causes

waveform distortion such first break delays (denoted throughout this paper as t_{fb}) correspond to neither phase nor group delays. Low-pass filtering can smooth signal onsets (Scherbaum 2002) and frequency-dependent attenuation and dispersion can cause pulse spreading and distortion (Wear 2000). This is especially relevant for fractures, because their frequency-dependent transmission characteristics create distorted waveforms. We demonstrate this discrepancy between first break, phase and group delays in the section 'Single Fracture Simulation Results'.

Quantification of Fracture Compliance

First we quantify the compliance of single fractures in the Discrete Particle Scheme model with quasi-static compression experiments. We denote these quasi-static fracture compliances as Z_{quasi}. They are obtained by building ratios between the observed vertical displacements across a fracture and the applied normal stress. Having established compliance values for the modelled fractures we then test several methods of quantifying fracture compliance from synthetic waveform data, that is from dynamic deformation. In ultrasonic laboratory experiments Pyrak-Nolte *et al.* (1990a) observed a systematic discrepancy between dynamic and quasistatic fracture compliance, possibly because of frictional effects. Toomey *et al.* (2002) however demonstrated that the properties of both compliances in the Discrete Particle Scheme are in agreement with linear-slip theory. One tested method

of quantifying fracture compliance is based on the determination of frequency dependent transmission coefficient curves from the waveforms and comparing them with analytical solutions. The other methods involve measuring different types of time delays from the waveform data and comparing them with the corresponding analytical solution. For the fracture set simulations we also use coda wave interferometry to derive time delays.

In the following we summarize the analytical solutions from linear-slip theory (Schoenberg 1980). In this theory a fracture is considered as an imperfectly bonded interface where the stress across the fracture is continuous but the displacement is discontinuous. The complex transmission and reflection coefficients T and R for a harmonic plane wave of angular frequency ω that propagates at normal incidence to a smooth, planar fracture with compliance Z embedded in a homogeneous, isotropic, linear elastic medium can be determined from equation 27 in Schoenberg (1980) as

$$T(\omega) = \frac{\frac{2}{\rho v Z}}{\frac{2}{\rho v Z} - i\omega} \tag{5}$$

$$R(\omega) = \frac{i\omega}{\frac{2}{\rho v Z} - i\omega} \tag{6}$$

where ρ is the rock density and v the compressional wave velocity. According to Pyrak-Nolte *et al.* (1987) the corresponding transmission coefficient modulus is

$$|T(\omega)| = \sqrt{\frac{\left(\frac{2}{\rho v Z}\right)^2}{\left(\frac{2}{\rho v Z}\right)^2 + \omega^2}} \tag{7}$$

This relationship defines the frequency dependent transmission of dynamic waves passing a fracture. As fractures in the Discrete Particle Scheme model comply with linear-slip theory (Toomey *et al.* 2002) curve matching between analytical and numerically derived transmission coefficient curves can be used to quantify fracture compliance.

Using the definition in equation 4 the group delay caused by a fracture with compliance Z can be expressed as (Pyrak-Nolte *et al.* 1987)

$$t_g(\omega) = -\frac{d\Theta(\omega)}{d\omega} = -\frac{d}{d\omega} arctan\Big(\frac{Im(T(\omega))}{Re(T(\omega))}\Big) = -\frac{d}{d\omega} arctan\Big(\frac{\omega\rho v Z}{2}\Big) = -\frac{\frac{2}{Z\rho v}}{(\frac{2}{Z\rho v})^2 + \omega^2} \tag{8}$$

This relationship is non-unique with respect to Z limiting the ability to uniquely infer fracture compliance from group delays, see Fig. 3. Deriving the corresponding phase delay t_{ph} we find that it is a unique function of compliance

$$t_{ph}(\omega) = -\frac{\Theta(\omega)}{\omega} = -\frac{1}{\omega} arctan\Big(\frac{Im(T(\omega))}{Re(T(\omega))}\Big) = -\frac{1}{\omega} arctan\Big(\frac{\omega\rho v Z}{2}\Big) \tag{9}$$

The compliance range displayed in Fig. 3 corresponds to observations in laboratory experiments. The phase delay t_{ph} increases monotonically with increasing fracture compliance whereas t_g reaches a maximum at a relatively low compliance of 0.22 x 10^{-13} m/Pa from which it tends to increasingly smaller group delays. For compliances around 2 x 10^{-13} m/Pa, t_{ph} is up to ten times larger than t_g.

In the case of strong scattering in a medium with multiple fractures, quantify-

ing time delays from signal envelopes or peak amplitudes does not perform well. We demonstrate that, in such cases, seismic coda can be used for relative fracture compliance determination, which is of interest for applications of monitoring temporal changes in compliance. The principles of the Coda Wave Interferometry method are outlined in the next section.

Coda Wave Interferometry

Coda Wave Interferometry is a technique for monitoring changes in a medium using elastic waves (Snieder 2002). The multiple scattering of wave energy in a medium generates wave trains, often called coda waves, that arrive after the direct arrivals. Coda waves are highly repeatable over time if a medium and the relevant source remain unchanged. However if a change in the scattering characteristics of the medium occurs, the waveform coda will change. Because the coda is composed of multiply scattered waves it samples the medium more effectively than the direct arrivals. This makes Coda Wave Interferometry a powerful tool for quantifying small velocity changes, e.g. caused by temporally varying fracture properties in the medium.

In a medium where repeated ”identical” sources are recorded with the same detector, velocity changes can be quantified by cross-correlating the two signals in moving time windows and plotting the lag-times of the resulting correlation

maxima versus time. For a uniform velocity variation the resulting slope is linear and proportional to the mean velocity change in the medium. Converting such velocity changes to time delays is straightforward for this study because the path length from source to receiver is precisely known. The technique has been successfully applied to ultrasonic laboratory experiments (Gret, Snieder and Scales 2006), volcano monitoring (Pandolfi, Bean and Saccorotti 2006) and several other applications (Snieder and Page 2007).

Single Fracture Simulation Results

Fracture Compliance from Transmission Coefficients

Many studies employ peak amplitude ratios to determine transmission or reflection coefficients of single fractures from dynamic waveforms (e.g. Cai and Zhao (2000); Toomey *et al.* (2002); Keiko *et al.* (2003); Lubbe *et al.* (2008)). These coefficients can then be compared with the analytical solution (equation 7) at the particular frequency of interest yielding a fracture compliance which we denote here as $Z_{amplitude}$. Table 1 lists $Z_{amplitude}$ values for three of our Discrete Particle Scheme simulations. They depart by about 5% from quasistatic Z_{quasi} values. This discrepancy arises because the source is not monochromatic. For comparison we derive fracture compliance values Z_{trans} for our non-monochromatic simula-

tions by matching observed transmission coefficients with the analytical solution, see Fig. 4. The transmission coefficient curves are obtained by dividing spectra of waveforms from fractured models by those from the unfractured model. There is an excellent fit between the analytical and the numerical curves demonstrating that the Discrete Particle Scheme models the frequency dependency of the transmission across single fractures in agreement with linear-slip theory. The obtained Z_{trans} values compare well with the Z_{quasi} values, see table 1.

Fracture Compliance from Time Delays

Group delays t_g are derived for the simulation data from the time intervals between envelope peaks of the waveforms from the intact and the fractured models, see Fig. 5. We find that t_g values only fit the analytical solution when waveforms are filtered in a narrow band around 1 MHz (0.97 to 1.03 MHz), see Fig. 6. We derive phase travel times by picking the largest positive peak of the waveforms and quantify phase delays t_{ph} by subtracting those from fractured models from those of intact models, see Fig. 5. While the resulting t_{ph} are only slightly smaller than those predicted by linear-slip solution, phase delays for waveforms filtered in a narrow band around 1 MHz (0.97 to 1.03 MHz) match the analytical solution better, see Fig. 6. The discrepancy between filtered and unfiltered delays is in accordance with the statement by Papoulis (1962) that the group and phase delay

concepts only apply correctly to narrowband signals.

We derive first break times by picking the onset times of the numerical signals. First break delays t_{fb} are calculated from the changes in first break times as caused by modelled fractures. The t_{fb} values depend somewhat on the zoom level used when picking signal onsets. Therefore we realize pickings at three different zoom levels and average these to obtain an error estimate. The t_{fb} values are found to match neither group nor phase delays. They increase monotonously with increasing compliance, similar to phase delays, see Fig. 6. The mismatch is to be expected as first break delays are only defined in the limit of infinite frequency, $t_{fb} = \lim_{\omega \to \infty} \frac{\Theta(\omega)}{\omega}$ (Papoulis 1962).

The analysis of group and phase delays demonstrates that single fractures modelled with the Discrete Particle Scheme have time delay characteristics agreeing with linear-slip theory and that the relationship derived for t_{ph} (equation 9) correctly describes phase delays in our simulations. It also shows that the expressions for t_g and t_{ph} (equation 8 and 9) only give correct group and phase delays when used for narrowband signals, though phase delays still give reasonably accurate results for broadband signals.

Fracture Set Simulation Results

In the physical world fractures often occur in clusters and cannot be treated in isolation. We employ the Discrete Particle Scheme to study the effect of five parallel, equally compliant, equidistant, effectively infinitely wide fractures on frequency-dependent wave transmission and time delays. Though such a configuration might not be realistic, fractures in rock masses often occur as sets of parallel fractures (Hsu and Schoenberg 1993). The simplification helps us to study the effects of fracture compliance and fracture spacing in isolation. The Discrete Particle Scheme, however, is capable of handling fractures of arbitrary size, orientation and spacing. We use models with fracture spacings of 0.08mm, 3.81mm and 11.43mm, in the following denoted as spacing 1, spacing 2 and spacing 3 (see Fig. 2). The dominant wavelength in the ”intact rock” areas in these models is 5.59mm and the fracture spacings correspond to 0.015, 0.68 and 2.05 wavelengths respectively. The observed frequency dependent transmission coefficients and time delays vary significantly between these models and the relationship between fracture spacing and wavelength is of paramount importance (see Fig. 7). For fracture spacings 2 and 3 multiple reverberations are observed and for fracture spacings 1 and 2 and the higher fracture compliance, pulse widening indicates diffusive wave propagation. At the smallest fracture spacing 1 and the lower fracture compliance the impact on the wave field is similar to that of a single fracture

(compare solid line in the bottom panel in Fig. 7 with Fig. 1).

Fracture Compliance from Transmission Coefficients

Ignoring the effect of multiple reflections the overall transmission coefficient $|T|$ of a set of n parallel fractures, each with individual transmission coefficient T_{ind}, is (Pyrak-Nolte, Myer and Cook (1990b); Cai and Zhao (2000))

$$|T| = |T_{ind}|^n \tag{10}$$

Nakagawa, Nihei and Myer (2000) termed this the T^n-method and showed that it is only valid when the first-arriving pulse is not contaminated by multiple reflections from within the fracture set. In agreement with this observation we find that only for the case of the largest fracture spacing, transmission coefficients agree with equation 10, see Fig. 8(a). For the two smaller fracture spacings, multiply reflected wave packages do interfere with the first pulse and consequently significant departures from the T^n solution are observed, see Fig. 8(b) and 8(c). The time window used for spectral analysis when determining the transmission coefficients is indicated by the double arrow in the top panel of Fig. 7. We tested the dependency of the transmission coefficients on the length of the time window and found that the main characteristics are preserved as long as the window does not overlap with strong reverbarations or the peg-leg multiples between the fractures and the model's boundaries.

Fracture Compliance from Time Delays

As already mentioned for the case of a single fracture, in practical terms time delays may yield a better estimate of compliance or compliance changes, than transmission coefficients. In the case of multiple fractures, for relatively small fracture spacings, transmission coefficient curves cannot be used to quantify the compliance of fracture sets, as demonstrated in the previous section.

Equivalent to the T^n method, ignoring multiple reflections in a fracture set yields a simple relationship for the overall group delay (Pyrak-Nolte *et al.* 1990b)

$$t_g = n \cdot t_{g_{ind}} \tag{11}$$

where n is the number of fractures and $t_{g_{ind}}$ the group delay caused by one individual fracture. The equivalent expression for the phase delay is

$$t_{ph} = n \cdot t_{ph_{ind}} \tag{12}$$

Because we study sets of five fractures, the time delay versus compliance curves are simply those for the single fracture experiments multiplied by five, see solid lines in Fig. 9 and 10 .

Group Delays

We find that it is not practical to filter the fracture set data in a narrow frequency band in order to test agreement with the analytical expression (equation 11) as we

did in the single fracture case. Even for the largest of the three fracture spacings the filtering causes envelopes of the individual reflections to widen so that no arrival time can be assigned to a "global maximum" of the first wave package envelope. Thus we compare only unfiltered group delays with the analytical solution. Figure 9 shows that, in disagreement with the analytical solution, group delays monotonously increase with increasing fracture compliance. For combinations of fracture spacing and compliance where no symbols are shown we could not pick envelope maxima because multiple reflection effects were too strong. Also shown in Fig. 9 are the group delays that one would expect ignoring multiple reflections for unfiltered data, i.e. corresponding values from the single fracture experiments multiplied by five (see solid triangular symbols). Only for the two larger fracture spacings and individual fracture compliances up to about 0.1 x 10^{-13} m/Pa group delays are similar to the analytical solution. In this compliance regime fracture stiffness is so high that multiple reflections play a minor role. Only in the case of the smallest fracture spacing multiple reflections are relevant at these high stiffnesses. Overall we find that group time delays measured from signal envelopes are not suitable for determining compliances for fracture sets.

Phase and First Break Delays

Filtering the data in a narrow frequency band, as in the case of the single fracture data, causes pulses to widen and overlap too much to permit the picking of

the largest positive peak. Even for unfiltered data peak amplitude picks are only practical for the largest fracture spacing and individual fracture compliances less than 0.5 x 10^{-13} m/Pa. Up to 0.25 x 10^{-13} m/Pa we find good agreement with the analytical solution (equation 12), see cross symbols in Fig. 10. We observe first break delays that monotonously increase with increasing fracture compliance, see unfilled symbols in Fig. 10. As expected first break delays are generally smaller than the analytical expression for t_{ph}. They follow the first break delays observed in the single fracture experiment quite closely when multiplied by 5, see filled triangles in Fig. 10. This suggests that the following expression for first break delays equivalent to equations 11 and 12 is useful for quantifying the overall first break delay in a fracture set

$$t_{fb} = n \cdot t_{fb_{ind}} \tag{13}$$

Coda Wave Interferometry Derived Delays

The previous sections demonstrate that it can be difficult to quantify time delays precisely for distorted, scattered signals. The Coda Wave Interferometry technique allows for a precise quantification of velocity perturbations, even if data are distorted by strong scattering. We investigate if deriving time delays with this technique can be used to infer fracture compliance in the numerical model with the large fracture spacing. Comparing Coda Wave Interferometry derived velocity changes with the time delays of this study is straightforward because the path

length from source to receiver is precisely known for the numerical model.

We find that waveforms from fractured and unfractured models are not similar enough to give sufficiently high cross-correlation values. However, if compliance differences are not too large, deriving velocity changes between two fractured models is possible. We plot the resulting velocity differences against the individual fracture compliance of the experiment with the higher compliance, see circular markers in Fig. 11. As a comparison we also show corresponding group and phase velocity differences from the unfiltered single fracture data after multiplying them by a factor of 5 (triangular and square symbols in Fig. 11). For fracture compliances of less than 0.4 x 10^{-13} m/Pa all three types of velocity changes are negative and the Coda Wave Interferometry delays follow the group delays more closely than the phase delays. For compliances larger than 0.4 x 10^{-13} m/Pa Coda Wave Interferometry and group velocity changes are very similar and positive, whereas phase velocity changes remain negative. This demonstrates that Coda Wave Interferometry velocity changes correspond to changes in group velocity rather than phase velocity. To compare with the analytical solution for group delays we convert the velocity change observed between two simulations with slightly different fracture compliance to a time delay difference. By adding the resulting delay difference to the analytical group delay of the simulation with the lower fracture compliance we obtain a group delay. Figure 12 shows that the resulting group delays fit well with the analytical solution.

Discussion and Conclusions

We test several methods of quantifying fracture compliance from ultrasonic data by comparing numerical data with analytical expressions. A main result is that for single fractures employing phase time delays is more practical than employing group delays or first break delays. We show that phase delays differ from group delays because the frequency dependence of the transmission across fractures causes waveform distortion. An analytical solution for phase delays based on linear-slip theory shows that phase delays are uniquely related to fracture compliance while group delays are not. In addition phase delays are less dependent on signal bandwith than group delays, see Fig. 6. We believe that these factors have hindered the wider application of deriving fracture compliance from travel times. Using phase delays could open new applications of fracture compliance quantification. First break delays mimic but do not match phase delay trends. This is a finite frequency effect. Hence first break delays cannot be compared to analytical solutions for compliance determination. They can, however, be compared to numerical simulations with appropriate source frequencies and known compliances.

Another method we test is to determine fracture compliance by comparing numerical and analytical transmission coefficients. We show that for broadband waveforms, deriving transmission coefficients simply from peak amplitudes does not yield accurate fracture compliances. Accurate compliances are obtained by

determining frequency-dependent transmission coefficient curves from waveform spectra and matching these with analytical solutions according to linear-slip theory.

While the discussion above relates primarily to isolated single fractures, field fractures rarely occur in isolation. Investigating the transmission characteristics of a set of parallel fractures we find, in agreement with previous studies, that they are highly dependent on the ratio between signal wavelength and fracture spacing. Observed transmission coefficients only agree with a simple analytical solution based on the T^n-method and linear-slip theory, if the first-arriving pulse is not contaminated by multiple reflections originating from within the fracture set. Thus deriving fracture compliance from transmission coefficients is limited to relatively large fracture spacings. We propose and test analytical expressions for group and phase delays analogous to the T^n-method. Observed group delays in our numerical data, measured from signal envelopes, do not match the analytical solution and are found to be unsuitable for quantifying fracture compliance. Phase delays only match the analytical solution if fracture spacings are large and compliances are relatively low. First break delays broadly follow the corresponding values of single fracture simulations after multiplying them by a factor corresponding to the number of identical fractures in the fracture set. Because first break delays are derived from the first arriving part of transmitted signals they are not effected by multiple reflections from within the fracture set. Thus first break delays allow

for an estimate of fracture compliance independent of fracture spacing. A priori numerical modelling of single fractures is required for such estimates.

Multiple fractures can often lead to highly distorted waveforms and coda generation. We test the application of the Coda Wave Interferometry method to derive time delays in the fracture set models. The advantage of this method is that it can be applied to heavily distorted waveforms and that absolute traveltimes do not need to be known to derive time delay changes. We find that quantifying absolute time delays relative to the unfractured model is only possible for very small fracture compliances. However, changes in time delays between models with higher fracture compliances can be quantified with the Coda Wave Interferometry method. We find a close match between Coda Wave Interferometry derived time delays and group delays, see Figs. 11 and 12. Because of the nature of group delays, Coda Wave Interferometry derived velocity changes can be positive or negative for an increase in fracture compliance. This means that in order to quantify the polarity of fracture compliance change using the Coda Wave Interferometry method, the pre-change absolute fracture compliance has to be estimated, e.g. from absolute velocities of the medium.

The methods considered in this work for quantifying absolute rock fracture compliance depend on the availability of data from an unfractured, comparable medium. In laboratory studies this can be achieved by comparing data from fractured and unfractured specimen. Well logs of single boreholes often provide data

from fractured and unfractured rock sections and in crosshole applications one can compare data from waves that traveled parallel and perpendicular to the primary direction of the fracture set under investigation (e.g. Myer *et al.* (1995); Lubbe and Worthington (2006)). For other cases the considered methods can still be used to infer changes in fracture compliance if the total value of fracture compliance is known. If none of this information is available the unique relationship between fracture compliance and phase delays can still be used in time-lapse studies to determine whether fracture compliance increases or decreases.

When employing the analytical expressions of linear-slip theory to quantify fracture compliance the actual range of the compliances plays an important role. For example, group and phase delays in this study are very similar for fracture compliances smaller than 0.1 x 10^{-13} m/Pa, see Fig. 6. The non-unique character of group delays plays no role at such small compliances. However, the fracture compliance range considered throughout this work is based on ultrasonic laboratory studies by other authors (see Fig. 3) and differences between group and phase delays are very relevant in this range.

The framework of linear-slip theory finds applications not only in ultrasonic studies, but also at sonic and seismic frequencies. It is therefore of interest to apply the methods tested in this work at these larger scales. Unfortunately only a few studies on quantifying in-situ rock fracture compliance exist (Worthington 2007). The compliances given in Worthington (2007) are used here to determine

the ranges of phase and group delays which one might expect at those scales. Figure 13 shows analytical phase and group delays at the scales of sonic cross-hole experiments (top panel), seismic reflection surveys (middle panel) and earthquakes (lower panel) assuming the same granite medium used in this study. Note the different ranges of time delay and fracture compliance for the different panels. The observed fracture compliance range at sonic frequencies is marked as an arrow and is relatively well constrained (Lubbe and Worthington 2006). The estimate of 1 x 10^{-9} m/Pa at the reflection seismic scale is less well constrained, see Worthington (2007). For the 5Hz scale we obtained an estimate of fracture compliance by simply extrapolating the linear plot of compliance versus fracture dimension in Worthington (2007). Because this linear relationship is far from verified this estimate has to be considered with caution. In all cases the significant difference between phase and group delay times comes into play. This points to the need for a clear understanding of how to extract phase, group and first break delay measures from recorded data.

Acknowledgments

Financial part support from the EU FP6 project 3HAZ, project number SSPI 004043, is acknowledged. We thank Gareth O'Brien for helpful discussions.

References

Cai J.G. and Zhao J. 2000. Effects of multiple parallel fractures on apparent attenuation of stress waves in rock masses. *International Journal of Rock Mechanics and Mining Sciences* **37**, 661–682.

Gret A., Snieder R. and Scales J. 2006. Time-lapse monitoring of rock properties with coda wave interferometry. *Journal of Geophysical Research* **111**, B03305, doi:10.1029/2004JB003354.

Hoover W.G., Ashurst W.T. and Olness R.J. 1993. Two-dimensional computer studies of crystal stability and fluid viscosity. *The Journal of Chemical Physics* **60**, No. 10, 4043–4047.

Hsu C.-J. and Schoenberg M. 1993. Elastic waves through a simulated fractured medium. *Geophysics* **58**, No. 7, 964–977.

Jaeger J.C., Cook N.G.W. and Zimmerman R.W. 2007. Wave propagation in rocks. In: *Fundamentals of Rock Mechanics* (ed. Jaeger, Cook and Zimmerman), Blackwell Publishing, ISBN 9780632057597.

Keiko Y., Sano O., Utada H., Takei Y., Nakao S. and Fukao Y. 2003. Long-term observation of in situ seismic velocity and attenuation. *Journal of Geophysical Research* **108**, doi:10.1029/2002JB002005.

Lubbe R. and Worthington M.H. 2006. A field investigation of fracture compliance. *Geophysical Prospecting* **54**, 319–331.

Lubbe R., Sothcott J., Worthington M.H. and McCann C. 2008. Laboratory estimates of normal and shear fracture compliance. *Geophysical Prospecting* **56** (2), 239247, doi:10.1111/j.1365-2478.2007.00688.x.

Myer L.R., Hopkins D., Peterson J.E. and Cook N.G.W. 1995. Seismic wave propagation across multiple fractures. In: *Fractured and Jointed Rock Masses* (ed. Myer, Cook, Goodman and Tsang), Balkema, Rotterdam, ISBN 9054105917.

Nakagawa S., Nihei K.T. and Myer L.R. 2000. Stop-pass behavior of acoustic waves in a 1D fractured system. *J. Acoust. Soc. Am.* **107** (1), 40–50.

O'Brien G.S. and Bean C.J. 2004. A 3D discrete numerical elastic lattice method for seismic wave propagation in heterogeneous media with topography. *Geophysical Research Letters* **31**, L14608, 10.1029/2004GL020069.

O'Brien, G.S. 2008. Discrete visco-elastic lattice methods for seismic wave propagation. *Geophysical Research Letters* **35**, L02302, doi:10.1029/2007GL032214.

O'Doherty R.F. and Anstey N.A. 1971. Reflections on amplitudes. *Geophysical Prospecting* **19**, 430–458.

Pandolfi D., Bean C.J. and Saccorotti G. 2006. Coda wave interferometric detection of seismic velocity changes associated with the 1999 M = 3.6 event at Mt. Vesuvius. *Geophysical Research Letters* **33**, L06306, doi:10.1029/2005GL025355.

Papoulis A. 1962. The Fourier Integral and Its Applications. *McGraw-Hill*, ISBN 0070484473.

Prioul R., Donald A., Koepsell R., El Marzouki Z. and Bratton T. 2007. Forward modeling of fracture-induced sonic anisotropy using a combination of borehole image and sonic logs. *Geophysics* **72**, No.4, E135–E147.

Pyrak-Nolte L.J., Cook N.G.W. and Myer L.R. 1987. Seismic visibility of fractures. *28th US Symposium on Rock Mechanics*, Tucson, 29 June – 1 July 1987, 47–56.

Pyrak-Nolte L.J., Myer L.R. and Cook N.G.W. 1990a. Transmission of seismic waves across single natural fractures. *Journal of Geophysical Research* **95**, 8617–8638.

Pyrak-Nolte L.J., Myer L.R. and Cook N.G.W. 1990b. Anisotropy in seismic velocities and amplitudes from multiple parallel fractures. *Journal of Geophysical Research* **95**, 11345–11358.

Scherbaum F. 2002. Analysis of Digital Earthquake Signals. In: *International*

Handbook of Earthquake and Engineering Seismology, Vol. 81A (ed. Lee, Kanamori, Jennings and Kisslinger), pp. 349–355. Int'l. Assoc. Seismol. and Phys. Earth's Interior. ISBN 0-12-440652-1.

Schoenberg M. 1980. Elastic wave behavior across linear slip interfaces. *J. Acoust. Soc. Am.* **68**, 1516–1521.

Schoenberg M. and Sayers M. 1995. Seismic anisotropy of fractured rock. *Geophysics* **60**, No.1, 204–211.

Snieder R. 2002. Coda wave interferometry and the equilibration of energy in elastic media. *Phys. Rev E* **66**, 046615, doi:10.1103/PhysRevE.66.046615.

Snieder R. and Page J. 2007. Multiple scattering in evolving media. *Physics Today* **60:55**, American Institute of Physics, 49-55.

Toomey A. and Bean C.J. 2000. Numerical simulation of seismic waves using a discrete particle scheme. *Geophysical Journal International* **141**, 595–604.

Toomey A., Bean C.J. and Scotti O. 2002. Fracture properties from seismic data - a numerical investigation. *Geophysical Research Letters* **29**, No. 4, doi:10.1029/2001GL013867.

Wear K. 2000. Measurement of phase velocity and group velocity in human calcaneus. *Ultrasound in Med. & Biol.* **26**, 4, 641–646.

Willis M.E., Burns D.R., Rao R., Minsley B., Toksoez M.N. and Vetri L. 2006. Spatial orientation and distribution of reservoir fractures from scattered seismic energy. *Geophysics* **71**, No. 5, 043–O51.

Worthington M. 2007. The compliance of macrofractures. *The Leading Edge* **26**, 1118–1122.

Zhang J. 2005. Elastic wave modeling in fractured media with an explicit approach. *Geophysics* **70**, No. 5, T75–T85.

Captions

Table 1

Fracture compliances derived for single fractures in the numerical model. $Z_{amplitude}$ is derived from peak amplitude ratios, Z_{quasi} from quasistatic compression simulations and Z_{trans} from transmission coefficients.

Figure 1

Sketch of the fracture implementation in the hexagonal lattice of the Discrete Particle Scheme. Dotted lines in the inset represent particle bonds that are more compliant than those in the unfractured rock matrix, represented by solid lines. A vertical planar source is input at the top surface of the model, the receiver location is indicated by the triangular symbol at the bottom. Infinitely wide boundary conditions are applied to the sides of the model to avoid interference effects. The snapshot represents the vertical displacement field in the numerical model after a wave front has been partly reflected by the horizontal fracture, see dashed line. The trace to the left represents a vertical slice through the snapshot.

Figure 2

Fracture spacings in the three multi-fracture numerical models and example snapshots of the vertical displacement field. Fracture spacings are 11.43x10^{-3}m (left,

"spacing 3"), 3.81x10^{-3}m (centre, "spacing 2") and 0.08x10^{-3}m (right, "spacing 1").

Figure 3

Fracture compliance dependency of phase and group delays (solid and dashed line respectively) for a signal frequency of 1MHz according to linear-slip theory. Phase delays are uniquely related to fracture compliance whereas group delays peak at 0.22 x 10^{-13} m/Pa. Compliance ranges measured by other authors in ultrasonic laboratory experiments are indicated by arrows.

Figure 4

Transmission coefficient curves as a function of frequency according to linear-slip theory (solid lines) and as determined from synthetic data (symbols). Error bars are smaller than the symbols.

Figure 5

Normalized displacement waveforms (solid lines) and their signal envelopes (dashed lines) for simulations with a single fracture. Fracture compliances Z are indicated on the left hand side of the figure. With increasing Z, phase arrivals are progressively delayed, see star symbols marking peak amplitude times. With increasing Z the maxima of the signal envelopes initially arrive later, but from about

Z=20x10^{-15} m/Pa they begin to arrive progressively earlier, see triangular symbols.

Figure 6

Phase and group delays measured from synthetic data, see triangular and square symbols respectively (unfilled: unfiltered data, filled: data filtered between 0.97MHz and 1.03MHz). First break delays are shown as star symbols. Analytical solutions of phase and group delays for a 1 MHz source are shown as solid lines. The errors for t_{ph} and t_g are smaller than the symbols in the figure.

Figure 7

Waveforms from numerical models with spacing 3 (upper panel), spacing 2 (centre panel) and spacing 1 (bottom panel). The compliances of the individual fractures are 4.3x10^{-15} m/Pa (solid lines) and 34.9x10^{-15} m/Pa (dashed lines). The double arrow in the top panel indicates the temporal window used throughout this paper for spectral analysis when determining transmission coefficients. The arrival at $\approx$ 3x10^{-5}sec, clearly visible in the bottom panel, is a peg-leg multiple between the fracture set and the top and bottom model boundaries.

Figure 8

Transmission coefficients determined from simulations with 5 parallel fractures with spacing 3 (a), spacing 2 (b) and spacing 1 (c). Analytical transmission coefficients according to the T^n method (see main text) are shown as solid lines. The compliances of the individual fractures are given in the legend.

Figure 9

Analytical group delays ignoring multiple reflections, for sets of 5 parallel fractures with individual compliance Z (solid line, equation 11). Unfilled symbols refer to group time delays derived from waveform envelope peak times. Filled symbols are group delays observed in single fracture experiments multiplied by 5.

Figure 10

Analytical phase delay (solid line) according to equation 12, which ignores multiple reflections, for sets of 5 parallel fractures with individual compliance Z. Phase delays (see cross symbols) can only be determined for fracture compliances below 0.5x10^{-13} m/Pa, see main text. First break delays are shown for all three fracture spacings as unfilled symbols. Filled symbols depict first break delays observed in the single fracture experiments multiplied by 5.

Figure 11

Velocity changes derived with the Coda Wave Interferometry method between multi-fracture models with varying fracture compliances (circular symbols). Expected group and phase velocity changes are derived from single fracture experiments by multiplication with 5 (triangular and square symbols respectively).

Figure 12

Absolute time delays in the fracture set model (circular symbols) derived by adding Coda Wave Interferometry derived delay differences to analytical group delays (dashed line), for details see main text.

Figure 13

Phase and group delays (solid and dashed lines respectively) according to the linear-slip theory for 23kHz (top panel, sonic frequency), 100Hz (centre panel, seismic reflection frequency) and 5 Hz (bottom panel, earthquake frequency). Arrows indicate estimates of absolute fracture compliance, see main text.

$Z_{amplitude}[10^{-15}\frac{m}{Pa}]$	$Z_{quasi}[10^{-15}\frac{m}{Pa}]$	$Z_{trans}[10^{-15}\frac{m}{Pa}]$
4.50 ± 0.04	4.33 ± 0.05	4.31 ± 0.01
33.47 ± 0.03	34.8 ± 0.05	34.85 ± 0.02
204.36 ± 0.05	214.3 ± 0.05	214.40 ± 0.04

Table 1: Fracture compliances derived for single fractures in the numerical model. $Z_{amplitude}$ is derived from peak amplitude ratios, Z_{quasi} from quasistatic compression simulations and Z_{trans} from transmission coefficients.

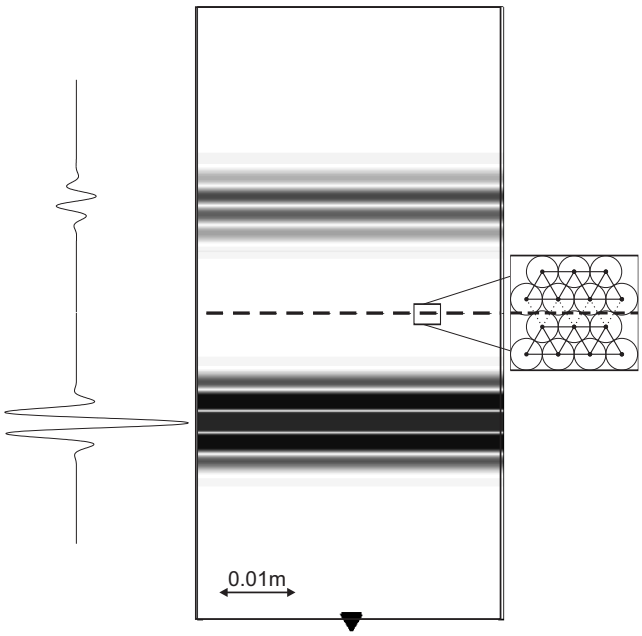

Figure 1: Sketch of the fracture implementation in the hexagonal lattice of the Discrete Particle Scheme. Dotted lines in the inset represent particle bonds that are more compliant than those in the unfractured rock matrix, represented by solid lines. A vertical planar source is input at the top surface of the model, the receiver location is indicated by the triangular symbol at the bottom. Infinitely wide boundary conditions are applied to the sides of the model to avoid interference effects. The snapshot represents the vertical displacement field in the numerical model after a wave front has been partly reflected by the horizontal fracture, see dashed line. The trace to the left represents a vertical slice through the snapshot.

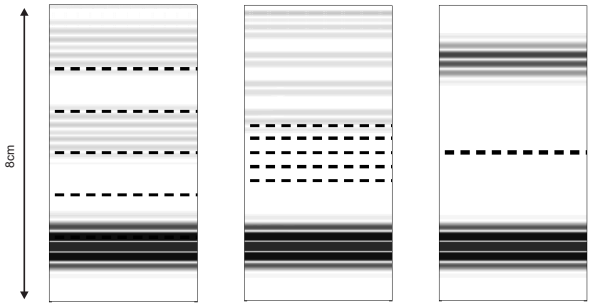

Figure 2: Fracture spacings in the three multi-fracture numerical models and example snapshots of the vertical displacement field. Fracture spacings are 11.43x10^{-3}m (left, ”spacing 3”), 3.81x10^{-3}m (centre, ”spacing 2”) and 0.08x10^{-3}m (right, ”spacing 1”).

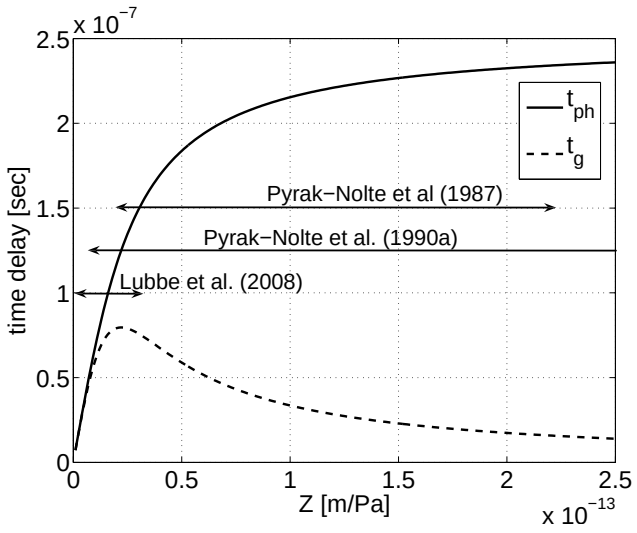

Figure 3: Fracture compliance dependency of phase and group delays (solid and dashed line respectively) for a signal frequency of 1MHz according to linear-slip theory. Phase delays are uniquely related to fracture compliance whereas group delays peak at 0.22 x 10^{-13} m/Pa. Compliance ranges measured by other authors in ultrasonic laboratory experiments are indicated by arrows.

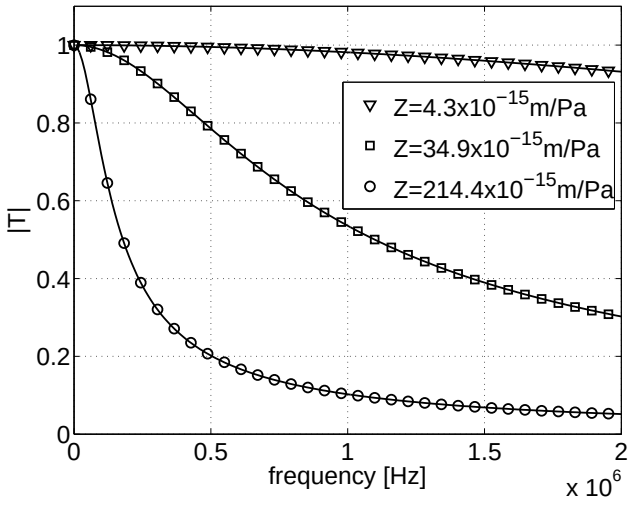

Figure 4: Transmission coefficient curves as a function of frequency according to linear-slip theory (solid lines) and as determined from synthetic data (symbols). Error bars are smaller than the symbols.

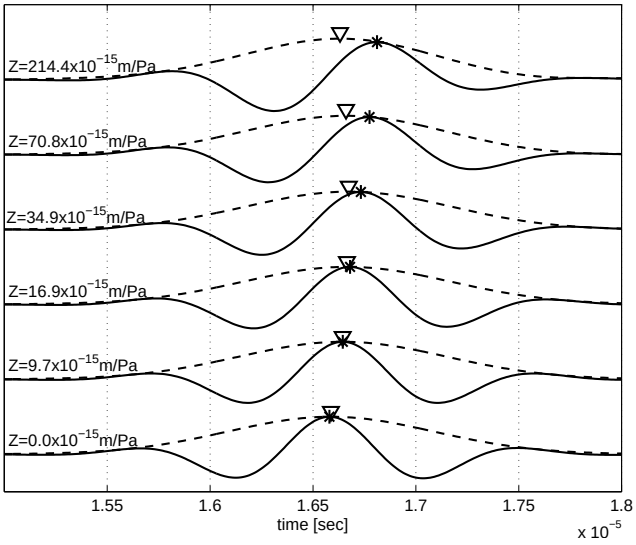

Figure 5: Normalized displacement waveforms (solid lines) and their signal envelopes (dashed lines) for simulations with a single fracture. Fracture compliances Z are indicated on the left hand side of the figure. With increasing Z, phase arrivals are progressively delayed, see star symbols marking peak amplitude times. With increasing Z the maxima of the signal envelopes initially arrive later, but from about Z=20x10^{-15} m/Pa they begin to arrive progressively earlier, see triangular symbols.

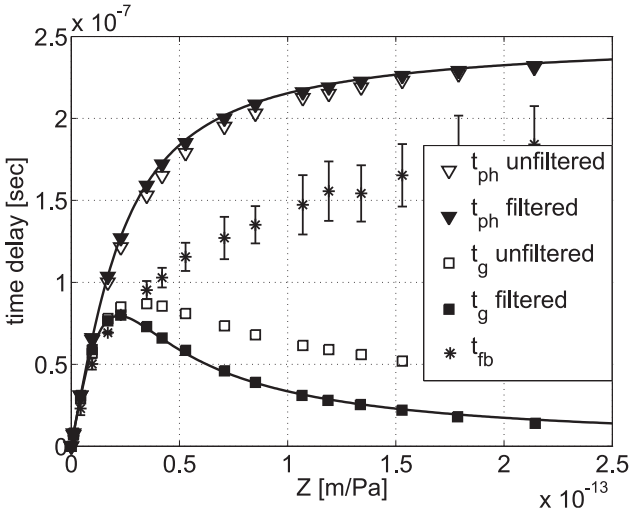

Figure 6: Phase and group delays measured from synthetic data, see triangular and square symbols respectively (unfilled: unfiltered data, filled: data filtered between 0.97MHz and 1.03MHz). First break delays are shown as star symbols. Analytical solutions of phase and group delays for a 1 MHz source are shown as solid lines. The errors for t_{ph} and t_g are smaller than the symbols in the figure.

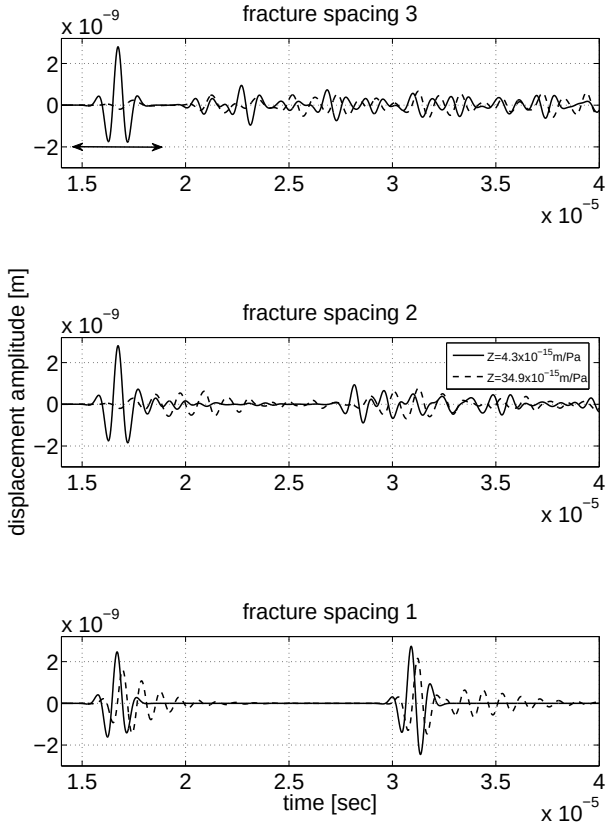

Figure 7: Waveforms from numerical models with spacing 3 (upper panel), spacing 2 (centre panel) and spacing 1 (bottom panel). The compliances of the individual fractures are 4.3x10^{-15} m/Pa (solid lines) and 34.9x10^{-15} m/Pa (dashed lines). The double arrow in the top panel indicates the temporal window used throughout this paper for spectral analysis when determining transmission coefficients. The arrival at $\approx$ 3x10^{-5}sec, clearly visible in the bottom panel, is a peg-leg multiple between the fracture set and the top and bottom model boundaries.

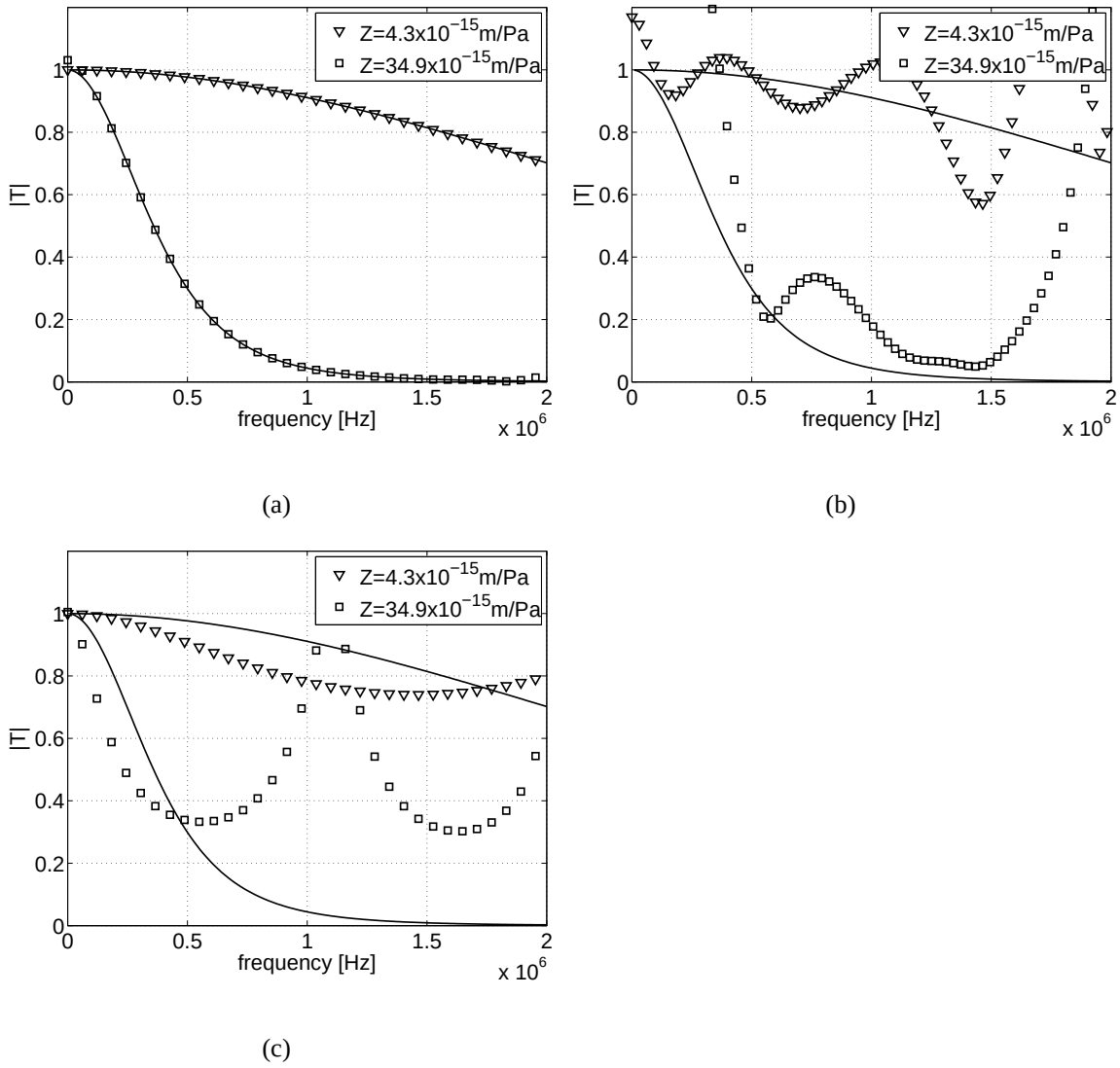

Figure 8: Transmission coefficients determined from simulations with 5 parallel fractures with spacing 3 (a), spacing 2 (b) and spacing 1 (c). Analytical transmission coefficients according to the T^n method (see main text) are shown as solid lines. The compliances of the individual fractures are given in the legend.

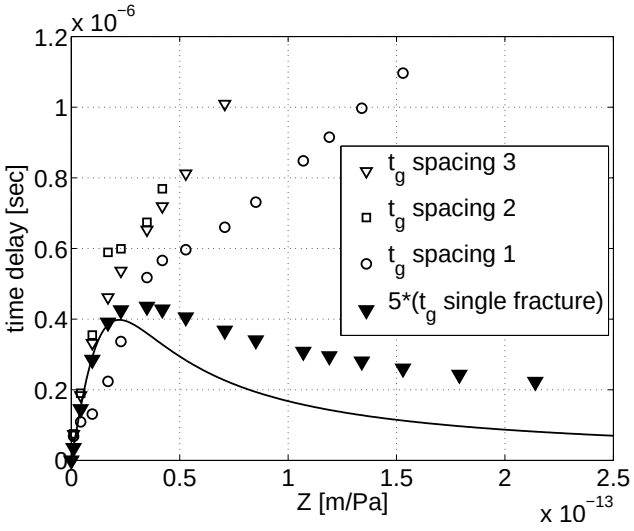

Figure 9: Analytical group delays ignoring multiple reflections, for sets of 5 parallel fractures with individual compliance Z (solid line, equation 11). Unfilled symbols refer to group time delays derived from waveform envelope peak times. Filled symbols are group delays observed in single fracture experiments multiplied by 5.

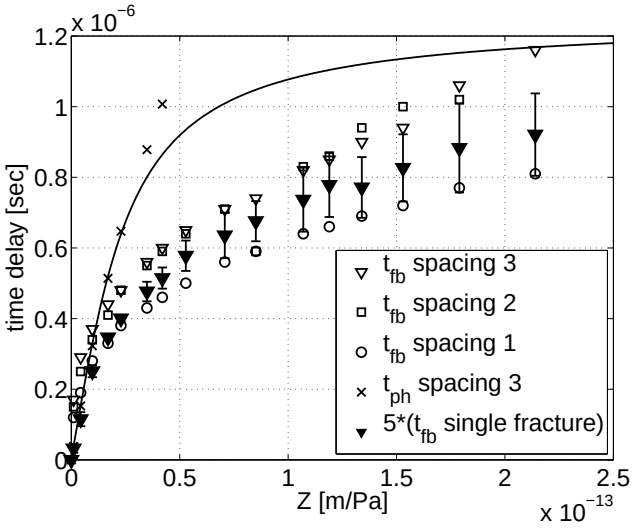

Figure 10: Analytical phase delay (solid line) according to equation 12, which ignores multiple reflections, for sets of 5 parallel fractures with individual compliance Z. Phase delays (see cross symbols) can only be determined for fracture compliances below 0.5x10^{-13} m/Pa, see main text. First break delays are shown for all three fracture spacings as unfilled symbols. Filled symbols depict first break delays observed in the single fracture experiments multiplied by 5.

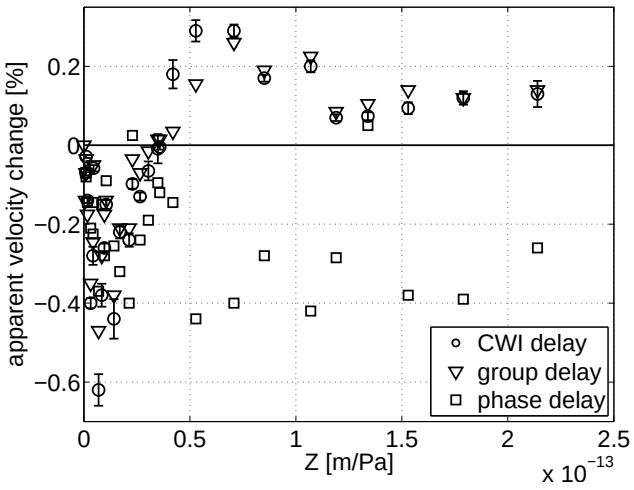

Figure 11: Velocity changes derived with the Coda Wave Interferometry method between multi-fracture models with varying fracture compliances (circular symbols). Expected group and phase velocity changes are derived from single fracture experiments by multiplication with 5 (triangular and square symbols respectively).

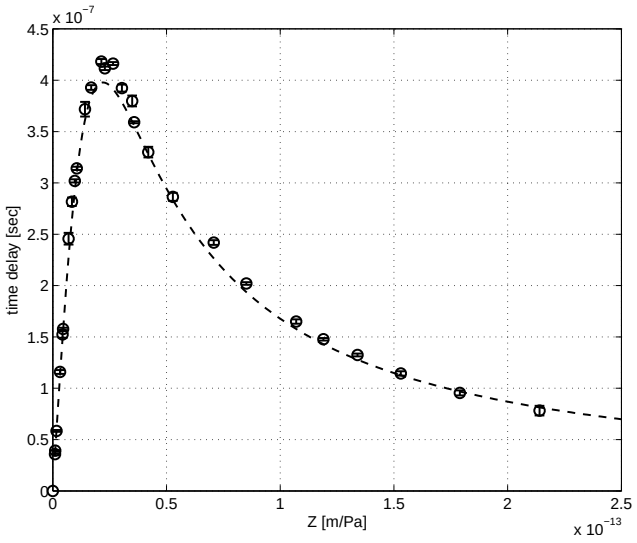

Figure 12: Absolute time delays in the fracture set model (circular symbols) derived by adding Coda Wave Interferometry derived delay differences to analytical group delays (dashed line), for details see main text.

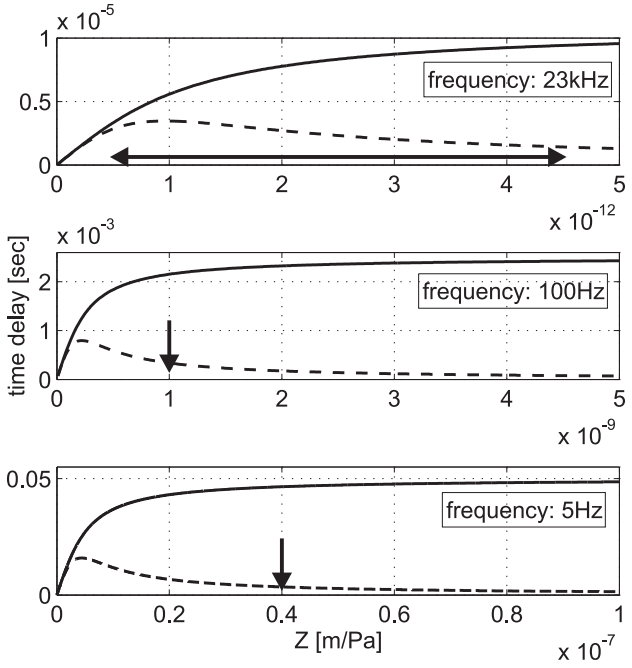

Figure 13: Phase and group delays (solid and dashed lines respectively) according to the linear-slip theory for 23kHz (top panel, sonic frequency), 100Hz (centre panel, seismic reflection frequency) and 5 Hz (bottom panel, earthquake frequency). Arrows indicate estimates of absolute fracture compliance, see main text.